Crystallization, melting and morphology of syndiotactic polypropylene fractions: 1. Thermodynamic properties, overall crystallization and melting*

Jonahira Rodriguez-Arnold, Anqiu Zhang and Stephen Z. D. Cheng†
Institute and Department of Polymer Science, College of Polymer Science and Polymer Engineering, The University of Akron, Akron, OH 44325-3909, USA

and Andrew J. Lovinger
AT&T Bell Laboratories, Murray Hill, NJ 07974, USA

and Eric T. Hsieh, Peter Chu, Tim W. Johnson, Kevin G. Honnell, Rolf G. Geerts, Syriac J. Palackal, Gil R. Hawley and M. Bruce Welch
Research and Development, Phillips Petroleum Company, Bartlesville, OK 74004, USA
(Received 26 July 1993; revised 15 November 1993)

A series of syndiotactic polypropylene (s-PP) fractions with constant syndiotacticities and different molecular weights have been studied through differential scanning calorimetry (d.s.c.), wide-angle X-ray diffraction (WAXD) and small-angle X-ray scattering experiments. The molecular weights, molecular weight distributions, syndiotacticities and sequence distributions of this series of fractions have been characterized by gel permeation chromatography, solution nuclear magnetic resonance and Fourier transform infra-red spectroscopy. The equilibrium melting temperature of sufficiently high molecular weight (above 40 000) s-PP with about 94% racemic dyads is $160 \pm 1°C$, and the heat of fusion is $8.0 \pm 0.3\ kJ\ mol^{-1}$. Overall crystallization rates exhibit a molecular weight dependence and a discontinuity with respect to crystallization temperature for the fractions. The temperature at which this discontinuity happens is at an undercooling of ca. 50°C. Based on nucleation theory, this discontinuity may be recognized as a regime III to regime II transition. With decreasing undercooling (increasing crystallization temperature) and molecular weight, a doubled crystal unit cell along the *b* axis becomes increasingly dominant during the crystallization. In this unit cell, opposite handedness of the helical chains exists along both the *a* and *b* axes (antichiral packing). Double melting peaks can be observed for all fractions in the high to middle undercooling region ($\Delta T > 50°C$), while only one melting peak can be found in the relatively low undercooling region. Different heating rate experiments after isothermal crystallization in d.s.c. and WAXD indicate that the low-melting crystal may undergo reorganization and melt-recrystallization processes to form the high-melting crystal. During this transformation, doubling of the crystal unit cell along the *b* axis with an antichiral packing of the chain molecules is obtained.

(Keywords: antichiral crystal; crystallization; syndiotactic polypropylene)

INTRODUCTION

Syndiotactic polypropylene (s-PP) was first synthesized and its configuration and conformation characterized by Natta *et al.*[1–4] in the 1960s. It was the first α-olefin polymer to be obtained in a highly regular, syndiotactic form. The syndiotacticity was studied by infra-red spectroscopy (i.r.) and nuclear magnetic resonance (n.m.r.) techniques[3,5–17].

The crystal structure and unit cell geometry of s-PP were determined by Natta *et al.*[1] from WAXD studies on oriented fibres. The unit cell was proposed to be orthorhombic with $a = 1.45$ nm, $b = 0.580$ nm (or $b = 0.560$ nm)[4], $c = 0.740$ nm and space group $C222_1$ (unit cell I). The crystallographic density was calculated to be $0.90\ g\ cm^{-3}$, slightly lower than the density of isotactic polypropylene ($0.936\ g\ cm^{-3}$). Along the *c* axis identity period, four monomer units are involved, and each unit cell contains eight units (two parallel chains). The chain adopts a two-fold helical form, $4 \times 2/1$, with a $(t_2g_2)_2$ conformation. Right-handed and left-handed helices are thus possible in s-PP chain molecules, and this may affect the crystal packing. In the lattice, the chain symmetry is fully maintained and packing depends on the bulkiness of the methyl groups. For a *C*-centred unit cell, chains of the same handedness are required. Therefore, the lattice is fully isochiral, with all molecules of the same handedness residing on *bc* sheets.

In the late 1980s, Lotz *et al.*[5] proposed an orthorhombic unit cell with $a = 1.45$ nm, $b = 0.560$ nm, $c = 0.740$ nm (unit

* Presented at 'International Polymer Physics Symposium Honouring Professor John D. Hoffman's 70th Birthday', 15–16 May 1993, Washington, DC, USA

† To whom correspondence should be addressed

0032-3861/94/09/1884–12

cell II) and a space group of $Pca2_1$ based on their electron diffraction (ED) results obtained from thin films of s-PP. Additional reflections and streaks on ED patterns from the single crystals produced by thin-film growth from the melt revealed features not reported in the fibre patterns studied previously by Natta's group. In this case, all the molecules are placed on the *ac* faces (face centred) rather than being *C*-centred. Strong evidence of a doubled cell along the *b* axis with $b = 1.120$ nm was recognized from three-dimensional electron diffraction analysis of s-PP single crystals in thin films. Further evidence for crystal doubling rests on an additional reflection peak at $2\theta = 18.8°$ in wide-angle X-ray diffraction (WAXD) patterns from bulk s-PP crystallized at high temperatures (racemic pentads >99%)[18,19]. This 'doubling' of the unit cell along the *b* axis is a consequence of a different packing scheme of the same chains. In the new unit cell symmetry, packing of both left-handed and right-handed helices is allowed, which will depend on the handedness of the depositing chain and those already on the crystal growth surface. Only chains with opposite handedness can be deposited on top of each other in a projection with a $c/2$ shift along the *c* axis. For unit cell II, alternating handedness is required along the *a* axis, while for unit cell III the chain packing must be antichiral along both the *a* and *b* axes. Furthermore, it has also been proposed that unit cell III is only found at high crystallization temperatures. With decreasing T_c, the incorporation of packing defects along the *b* axis has been identified[20,21].

Recently, Lovinger *et al.*[20] investigated the temperature dependence of the s-PP (racemic dyad content of 0.769 and syndiotactic and isotactic triad fractions of 0.698 and 0.159, respectively) crystal morphology and its epitaxial relationship with i-PP. At the highest crystallization temperature region ($T_c > 105°C$) large, rectangular, and highly regular single crystals were observed by phase-contrast light microscopy. These crystals had the same new (antichiral) unit cell and interchain packing as previously observed[5]. As T_c was decreased the morphology became axialitic and eventually spherulitic (in the vicinity of $T_c = 70°C$). It was suggested that in this lower crystallization temperature region intermolecular packing disorder with both handednesses is introduced owing to kinetic considerations in the crystallization process. Overgrowths observed by transmission electron microscopy (TEM) on the s-PP crystals were also identified as individual i-PP crystals. This phenomenon was believed to be initiated by a specific epitaxial relationship with the lateral surfaces of s-PP lamellae. At higher syndiotacticity levels, it seems that s-PP shows a very similar behaviour to that of relatively low syndiotacticity samples, but the temperature correspondence with crystal structure and morphology shifts about 40°C towards the higher temperature side[18–23].

The helical conformation of s-PP chains is the most stable. However, an unstable form was also observed by Turner-Jones and Cobbold[24] and Natta *et al.*[25] consisting of planar zigzag polymer chains. The samples were obtained by the cold drawing of polymer quenched from the melt. The helical form was completely absent. Upon annealing at about 100°C the samples were converted from the planar zigzag to the helical form. In more recent work[26] a *c* axis (fibre direction) of 0.505 nm in a planar zigzag form was identified. From WAXD fibre patterns an orthorhombic unit cell of $a = 0.522$ nm, $b = 1.117$ nm and $c = 0.506$ nm was determined. Assuming that four monomer units are contained in each unit cell, the calculated crystallographic density was 0.945 g cm^{-3} (the observed density is in the vicinity of 0.885 g cm^{-3}). The crystallite size in this quenched form was extremely small, approximately a few nanometres.

In some of the WAXD fibre patterns a reflection indicating a periodic *d* spacing of about 0.28 nm or a multiple of this value suggested the existence of a third crystalline phase. Chatani *et al.*[27] reported a new crystalline form, a triclinic lattice of $a = 0.572$ nm, $b = 0.764$ nm, $c = 1.16$ nm, $\alpha = 73.1°$, $\beta = 88.8°$ and $\gamma = 112.0°$, with a space group of $P1$. The crystallographic density was calculated to be 0.939 g cm^{-3} where six monomer units are included, while the observed density was in the vicinity of 0.89 g cm^{-3}. The chain does not have centres of symmetry. The two conformations suggested are formed either by deforming the $(ttgg)_2$ helix resulting in a chain repeat of three (ttgg) in two turns of the helix, or alternatively through a $(t_6g_2t_2g_2)$ conformation. The latter was considered as an intermediate state between planar zigzag and helical forms. As with the planar zigzag form, this third crystalline phase may be transformed into the helical form by annealing above 50°C[27].

The thermodynamic properties of s-PP crystals in the high temperature orthorhombic form have been reported by several authors. The T_m° was estimated to be in the range 140–170°C by Boor and Youngmann[13]. Values of 151°C and 155°C for s-PPs with relatively short sequences were published by Haftka and Konnecke[12]. Miller and Seeley determined a T_m° of 158.8°C using the Hoffman–Weeks method which utilizes observed T_m *versus* T_c extrapolation[28]. Based on the syndiotacticity information and using the conditional probabilities and the Flory theory for the depression of melting temperature in copolymers[29], they predicted that for 100% s-PP the equilibrium melting temperature should be around 220°C. A calculated ΔH_f° of about 1.88 kJ mol^{-1} was obtained assuming amorphous and unit cell densities of 0.854 and 0.90 g cm^{-3}, respectively[11,13]. The higher end value of the ΔH_f° was reported to be 8.26 kJ mol^{-1} using WAXD and d.s.c. data[12]. No equilibrium thermodynamic property data are available for the low temperature, quenched orthorhombic and triclinic crystal forms owing to their thermodynamic metastability.

The crystal melting behaviour of s-PP has been reported to show heating and cooling rate dependencies[5,11,30,31]. Two melting peaks were observed and attributed to different thermodynamic stabilities of the crystals. It was found that the low-melting peak always contributes a larger portion of the heat of fusion at relatively fast heating rates. However, there has not been a systematic study of s-PP crystal melting at different crystallization temperatures and times as well as heating rates. Very little structure correlation has been proposed associated with these two melting peaks.

Finally, in the study of s-PP, it is important to recognize the syndiotacticity effects on crystallization, crystal melting and morphology. These have been demonstrated in the recent investigations reported by Lovinger, Lotz and others (high racemic pentads *versus* relatively lower racemic pentads)[5,18–23]. The sequence distribution of the syndiotactic components in s-PP also affects these properties, as in the case of vinyl polymers.

In this publication, as the first part of this series, we focus on the sample characterization, in particular the

Table 1 Molecular parameters of syndiotactic polypropylene fractions

Sample	$10^{-3}M_n$	M_w/M_n	[r][a] (%)	[rr][b] (%)	[rrrr][c] (%)	Block m[d]	Block r[e]
s-PP(1)	10.3	1.2	94	91	85	1.85	28.9
s-PP(2)	15.5	1.1	94	91	86	1.84	30.7
s-PP(3)	20.8	1.1	95	93	88	1.81	37.8
s-PP(4)	26.2	1.1	94	91	86	1.83	34.0
s-PP(5)	33.3	1.1	94	92	86	1.83	34.1
s-PP(6)	41.7	1.1	94	92	86	1.84	31.7
s-PP(7)	53.2	1.1	94	92	86	1.84	31.7
s-PP(8)	76.8	1.1	94	92	86	1.84	31.7
s-PP(9)	132	1.2	95	92	87	1.83	33.9
s-PP(10)	234	1.2	95	92	87	1.77	34.1

[a] Racemic dyads [r]
[b] Triads [rr]
[c] Pentads [rrrr]
[d] Number-averaged isotactic block, $2([mm]+\frac{1}{2}[mr])/[mr]$
[e] Number-averaged syndiotactic block, $2([rr]+\frac{1}{2}[mr])/[mr]$

syndiotactic structure of the fractions. The overall crystallization, melting and thermodynamic properties of s-PP crystals grown from these s-PP fractions are reported.

EXPERIMENTAL

The polymer materials examined in this study were narrow molecular weight distribution (*MWD*) s-PP fractions prepared and characterized in the Research and Development department of Phillips Petroleum in Bartlesville, OK. These fractions were similar in molecular stereoregularity and differed only in molecular weight (*MW*). The syndiotactic dyad sequence molar concentrations (i.e. [r], as measured by solution n.m.r.) for most of these fractions were around 94–95%, and the polydispersity values were typically 1.1–1.2. Detailed molecular characteristics of these fractions are listed in *Table 1*.

The fractions were derived from a parent polymer made with a homogeneous metallocene catalyst. The fractionation method, which will be detailed elsewhere, was a variation of the 'successive extraction' fractionation method[32]. In order to gather sufficient material in each fraction for analyses, three fractionation runs had to be performed. Each run started with 15 g of the same parent polymer, and resulted in 15 fractions following the same experimental procedure. Comparisons of weight per cent polymer recovered in 'matching fractions' (i.e. fractions obtained under the same dissolution conditions from separate runs) indicated very good reproducibility among the three fractionation experiments.

Gel permeation chromatography (g.p.c.; Waters 150CV) was performed on all fractions. Results again indicated that matching fractions had statistically equivalent *MW* and *MWD* characteristics. It is thus concluded that matching fractions from the three separate runs contained essentially the same collection of molecular components. To maximize the usage of the limited amounts of materials available, nuclear magnetic resonance (n.m.r.) analyses were done on one of the three series of fractions only. Materials from the other two runs were dedicated to the crystallization study detailed in this report. The following is a summary of the experimental conditions used in our g.p.c. and n.m.r. analyses.

The g.p.c. instrument was a Waters 150CV operated at 140°C. 1,2,4-Trichlorobenzene (TCB) was the eluent and the solvent. The antioxidant employed was Topanol CA at a level of 0.5 g l^{-1}. The flow rate was 1 cm^3 min^{-1}, and the injection volume was typically 220 μl. The column configuration consisted of two Waters Styragel HT 6E columns in series. To minimize artificial peak broadening and other related artefacts, the sample solution concentration was kept at no more than 1.5 mg of polymer per 3.5 cm^3 of solvent. The columns were calibrated for every carousel of 16 runs using a broad *MWD* polyethylene second standard. Mark–Houwink constants for isotactic polypropylene were used for calculating the molecular weights. No attempt was made to determine whether s-PP should have a different set of Mark–Houwink constants.

The ^{13}C n.m.r. spectra were recorded on a Varian Unity 500 at 125.7 MHz. The instrumentation conditions were as follows: temperature 125°C; pulse angle 90°; pulse delay 5 s; acquisition time 3 s; spectral width 8000 Hz; number of data points per spectrum 48 K; and broad band decoupling and double precision were enabled during the data acquisition. Polymer sample solutions were prepared in TCB at about 10 wt% if there was enough polymer material. Deuterated benzene was added as internal lock solvent. No internal standard for chemical shift reference was used. About 5000 transients were taken for each spectrum. Various stereoregularity parameter values were derived from the integrals of the methyl carbon peaks. Since all of the methyl carbons have about the same T_1 (for PP molecules in dilute solution) regardless of their configurational environment, the relatively short pulse delay employed in this particular instance had no effect on the accuracy of the tacticity information derived using only the methyl carbon peak intensities. The number-averaged isotactic and syndiotactic blocks were calculated based on the expressions included in *Table 1*.

Fourier transform infra-red spectroscopy (*FT*i.r.; Galaxy 5200) was used to identify any possible isotactic content in the fractions in the wavenumber region

between 400 and 4000 cm^{-1}. The fingerprint wavelengths of syndiotactic components are 7.62, 7.91, 9.94, 11.53 and 12.32 μm based on the findings of Natta *et al.*[1]. The isotactic components[1] possess the fingerprint wavelengths of 7.66, 7.96, 10.03 and 12.36 μm.

Differential scanning calorimetry (d.s.c.) experiments were carried out on a Seiko DSC220. The temperature and heat flow scales were carefully calibrated at different heating rates (1.0°C min^{-1} to 40°C min^{-1}) using standard materials in the temperature range studied. The sample weight was typically about 2–3 mg at a heating rate of 10°C min^{-1}. With increasing heating rates, the sample weight was correspondingly decreased to avoid superheating. For example, a sample weight of less than 0.2 mg was used when the heating rate was 40°C min^{-1}. Isothermal crystallization experiments were performed by transferring as quickly as possible the samples from a hot stage at 180°C to the d.s.c. with a preset isothermal temperature. After complete crystallization, the samples were heated up to above the melting temperature with and without prior cooling to room temperature. When thermograms during heating showed two melting peaks, a peak separation procedure was adopted using a computer program. This program was utilized under the assumption of an asymmetric double sigmoidal function at the preconditions for the number of peaks and the positions of their maxima.

Wide-angle X-ray diffraction (WAXD) experiments were carried out using a Rigaku 12 kW rotating anode generator and diffractometer operated in the reflection mode. A home-built temperature controller used on the WAXD equipment with an accuracy of ± 1°C in the temperature region studied. Isothermal crystallization and heating at a constant rate (0.5–5°C min^{-1}) were conducted after completion of the crystallization of these s-PP fractions, and the time-resolved crystallization, annealing and melting behaviours were followed. The monochromatized X-ray beam was CuKα radiation with a wavelength of 0.15438 nm. In order to obtain crystallinity from WAXD experiments, an amorphous background is needed. This background was constructed through measurements of s-PP samples at elevated temperatures between 150 and 180°C, and these data were then extrapolated to the different temperatures at which isothermal crystallization experiments were carried out. Such extrapolation only takes the coefficient of thermal expansion into account as a first approximation. To calculate the apparent crystal sizes of the different crystalline planes, the Scherrer equation was used based on the widths at half height of the reflection peaks calibrated via standard silicon crystals.

Time-resolved synchrotron, small-angle X-ray scattering (SAXS) experiments were carried out on the Oak Ridge National Laboratory beam line X-14 of the National Synchrotron Light Source (NSLS). The detailed instrumental set-up has been described in a previous publication[33]. In brief, the X-ray wavelength was 0.15498 nm (8.000 keV) and the beam was focused through a dynamically bent Si crystal monochromator with a beam size of 0.1×1.0 mm ($V \times H$) at the sample location. A position sensitive proportional counter (Ordella 1020) was used to record the scattering patterns. A customized temperature-jump hot stage was built and situated on a Huber goniometer for isothermal measurements. The temperature of this hot stage was calibrated with standard materials during the beam irradiation. The precision of the temperature controller was ± 1°C. The lamellar thickness was obtained by using a correlation function method[34].

RESULTS

Molecular characterization of s-PP fractions

Based on g.p.c., n.m.r. and *FT*i.r. experiments, the number-average molecular weights, polydispersities, syndiotacticities from racemic dyads [r] up to pentads [rrrr], and number-averaged isotactic and syndiotactic blocks were determined (see *Table 1*). It is evident that these fractions all possess the same syndiotacticities of $94 \pm 1\%$ in terms of dyads [r] and $86 \pm 1\%$ in terms of pentads [rrrr]. The n.m.r. results show that the fractions do not have a wide spread of syndiotacticity amongst the constituent molecules. The *FT*i.r. spectra showed no detectable isotactic content. It should be understood that for isotactic polypropylene two kinds of mistakes regarding isotacticity may be identified. The first type of mistake is caused by catalysts in which two consecutive racemic conformations [rr] are needed to correct the mistake. The second type of mistake is the end-chain mistake, since only one racemic conformation [r] is needed, followed by a change of *d* and *l* helices. The crystallization behaviour of the i-PP fractions is critically dependent upon the run length in the chain molecules between two neighbouring defects[35–38]. The tacticity mistakes in s-PP should be illustrated in a similar way. In fact, in this series of s-PP fractions, the majority of defects were introduced by catalysts with a pair of [mm] defects[38]. This fact is also demonstrated by the number-averaged isotactic blocks (*Table 1*), which are close to 1.8 or above for all the fractions (if this value is 2, all the defects must be of [mm] type).

Overall crystallization

Overall crystallization behaviour can be studied using the Avrami treatment of data obtained from d.s.c. experiments. *Figure 1* illustrates the relationship between $\log[-\ln(1-w^c)]$ and crystallization time ($\log t_c$) for two s-PP fractions (s-PP(3) and s-PP(10)) at different temperatures. For all the fractions, the slopes (dimensionality parameter, *n*) range from 1.9 to slightly over 3.0 for the primary crystallization process. A second crystallization process is clearly seen in the final stages of growth with a lower slope (*Figure 1*). This process is always observed after the impingement of the crystal entities, representing a further development of the crystallinity within the entities on a finer scale. However, the Avrami treatment needs to be associated with detailed morphological studies, otherwise it represents only a convenient overall data representation. Polarized light microscopy observations indicated that a heterogeneous nucleation was the main process in this crystallization temperature region. Such morphological studies are now being conducted, and the results will be reported in the second part of this series of publications. At this moment, we focus on the relationship between crystallization time at 10% development of the overall crystallinity and crystallization temperature. The two detailed quantities in the plot are $\log(1/t_{0.1}) - \log(\Delta T) + U^*/2.303R(T_c - T_\infty)$ and $1/T_c(\Delta T)f$, as shown in *Figure 2* for s-PP(3), s-PP(7) and s-PP(10), where ΔT is the undercooling, $t_{0.1}$ is the crystallization time at which 10% of the overall

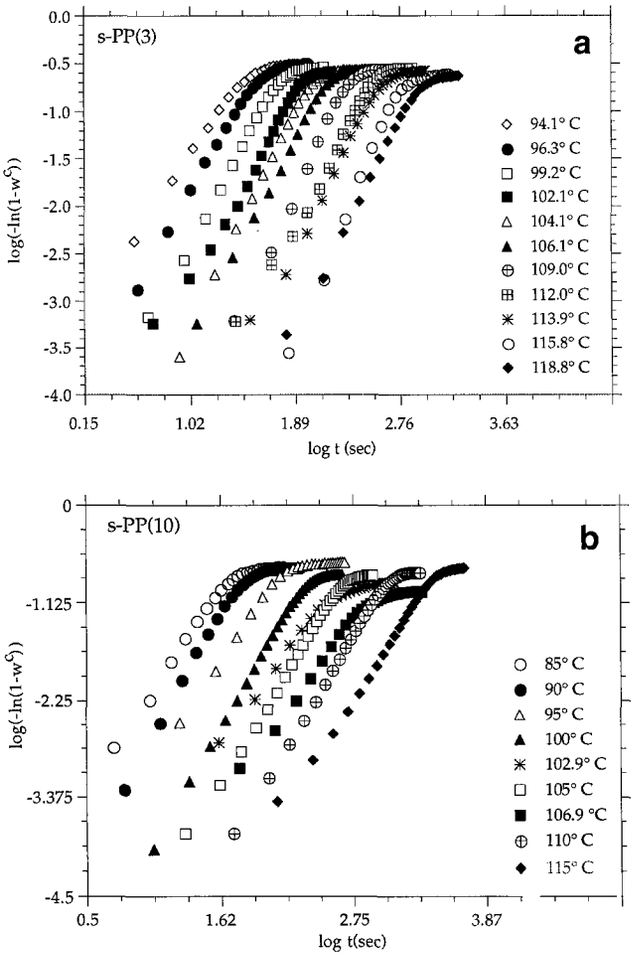

Figure 1 Avrami treatments of (a) s-PP(3) and (b) s-PP(10) at different temperatures

crystallinity is developed, $U^* = 6.28\ \text{kJ mol}^{-1}$ is the universal transport energy term[38], R is the gas constant, $f = 2T_c/(T_m^\circ + T_c)$, and $T_\infty = T_g - 30°\text{C}$. (The T_m° for s-PP(3) is 158°C, and other two fractions possess the same T_m° of 160°C; see below.) This plot is traditionally based on the nucleation theory of polymer crystallization[39–43]. It is interesting that for each fraction a discontinuity in the slope at a certain crystallization temperature can be found. This temperature corresponds well to a constant undercooling of about 50°C for the fractions. The ratio between the two slopes in *Figure 2* is close to 2 (i.e. a ratio of 2.1 for s-PP(3), 1.9 for s-PP(7) and 2.2 for s-PP(10)), as would be expected for a regime transition.

Crystal melting

Figure 3 shows a set of d.s.c. heating curves at a heating rate of 10°C min^{-1} for s-PP(7) fractions after isothermal crystallization at different temperatures. It is evident that with increasing temperature (decreasing undercooling) the overall heat of fusion slightly increases. Moreover, two melting peaks are always seen when the crystallization temperature is below 105°C. The low-melting peak shows a clear dependence on crystallization temperature (undercooling), while the high-melting peak is almost constant. In this temperature region, with increasing crystallization temperature the low-melting peak increases its share of the heat of fusion $\Delta h_f(l)$. This observation can be represented by a ratio between the heats of fusion of the low-melting and high-melting peaks, i.e. $\Delta h_f(l)/\Delta h_f(h)$, as shown in *Figure 4* for s-PP(3), s-PP(6) and s-PP(10) fractions. For all the fractions, this ratio increases with T_c. Moreover, at the same temperature, the value of this ratio increases with molecular weight. Above a certain T_c (in the case of s-PP(7), for example, $T_c = 105°\text{C}$; see *Figure 3*), only one endothermic melting peak is observed. Further increase in T_c only leads to an

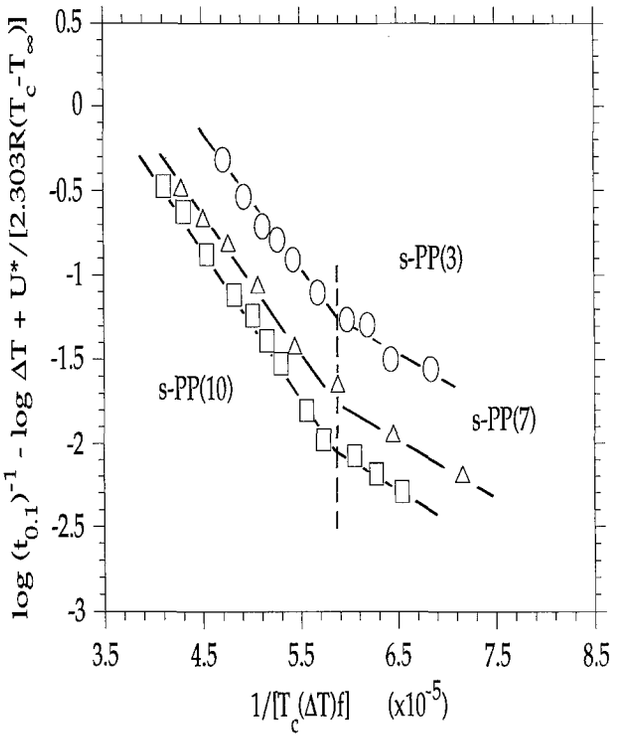

Figure 2 Relationships between $\log(1/t_{0.1}) - \log(\Delta T) + U^*/2.303R(T_c - T_\infty)$ and $1/T_c(\Delta T_f)$ for s-PP(3), s-PP(7) and s-PP(10) (the equilibrium heats of fusion and melting temperatures are from *Figures 12* and *13*)

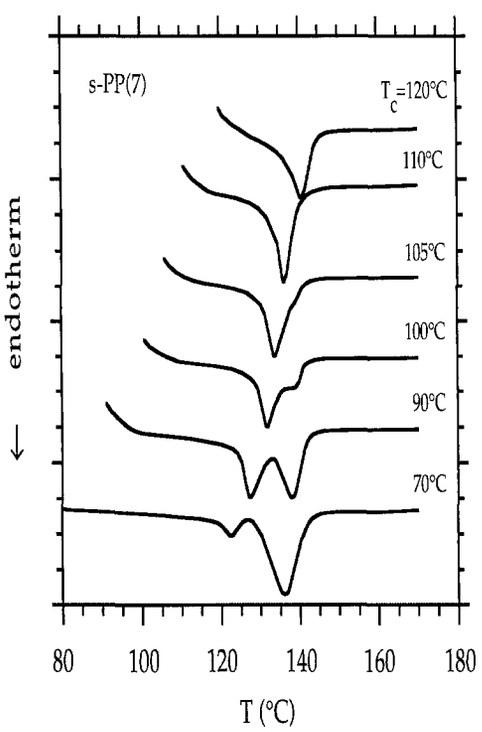

Figure 3 Set of d.s.c. heating curves (heating rate of 10°C min^{-1}) for s-PP(7) fractions crystallized at different temperatures

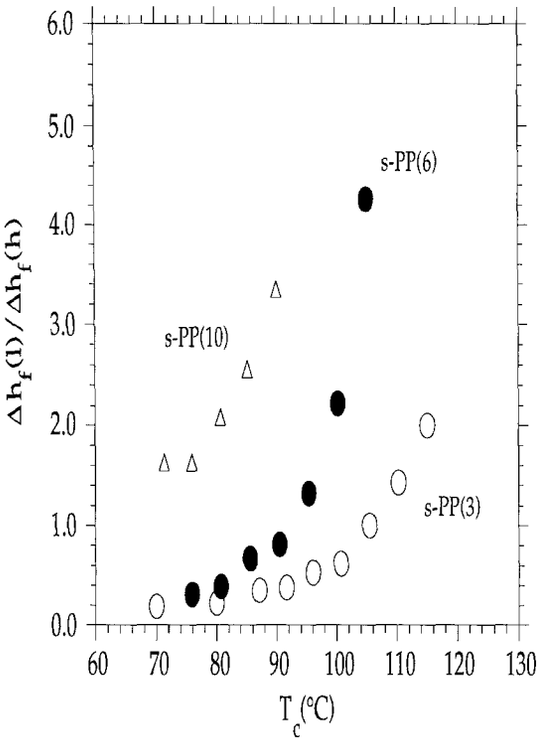

Figure 4 Relationships between the ratio $\Delta h_f(l)/\Delta h_f(h)$ and crystallization temperature for s-PP(3), s-PP(6) and s-PP(10) at a heating rate of 10°C min^{-1}

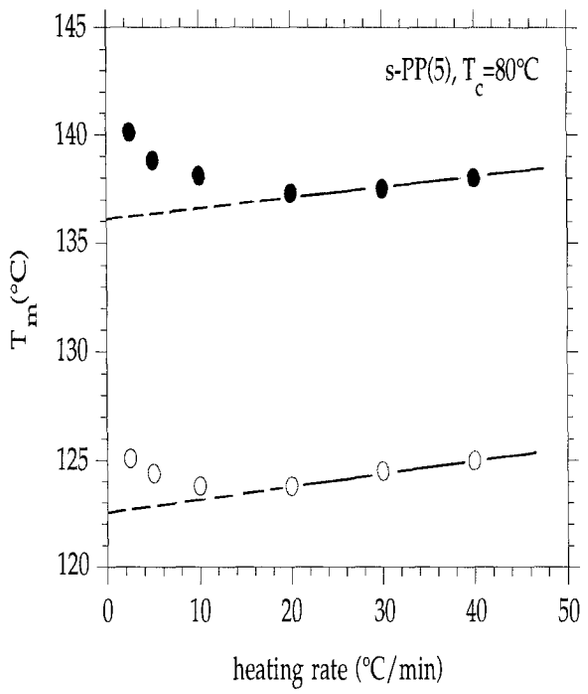

Figure 5 Relationship between melting temperature and heating rate for s-PP(5) crystallized at 80°C: (○) low-melting peak; (●) high-melting peak

increase in the melting temperature of this peak. This phenomenon has been observed for all the fractions studied. With increasing molecular weight, the crystallization temperature above which the two-melting-peak phenomenon disappears decreases. For example, the s-PP(3) fraction exhibits two melting peaks below $T_c = 115$°C, while for s-PP(10) a 90°C transition is seen.

Different heating rates were used after the sample was completely crystallized at a T_c prior to cooling. Changes of the temperatures of these two melting peaks with heating rate below a certain T_c are shown in *Figure 5* for s-PP(5) as an example. Both the melting temperatures decrease at first with increasing heating rate, reach minima at a heating rate of ca. 20°C min^{-1} or slightly faster, and increase again at even faster heating rates. It is evident that the higher melting temperatures at the slow heating rate are due to an annealing effect during heating. Above the heating rate of 20°C min^{-1}, the increase of the melting temperature may be caused either by crystal superheating or by the instrumental thermal lag. To distinguish between these two effects, one may use a plot of the difference between the peak and the beginning of the melting endotherm *versus* the square root of the heating rate, as proposed by Illiers some years ago[44]. We find that this relationship is linear, indicating that this increase of the melting temperature with heating rate is caused by the instrumental thermal lag and not by crystal superheating. Consequently, an extrapolation can be made to 0°C min^{-1} from the melting temperatures of the fast heating rate side to obtain a melting temperature which should approximate the true melting temperature of the crystal formed at T_c without any annealing effect (dashed lines in *Figure 5*). Other fractions also show a similar behaviour as described here.

Figure 6 shows the relationships between the heats of fusion of the individual melting peaks and the logarithmic heating rate for s-PP(8) after isothermal crystallization at 80°C. It is evident for both melting peaks that apparent linear relationships exist. With increasing heating rate, the heat of fusion of the low-melting peak increases, while that of the high-melting peak decreases. This clearly indicates an annealing effect during heating. D.s.c. experiments were also conducted by holding the temperature between the two melting peak temperatures

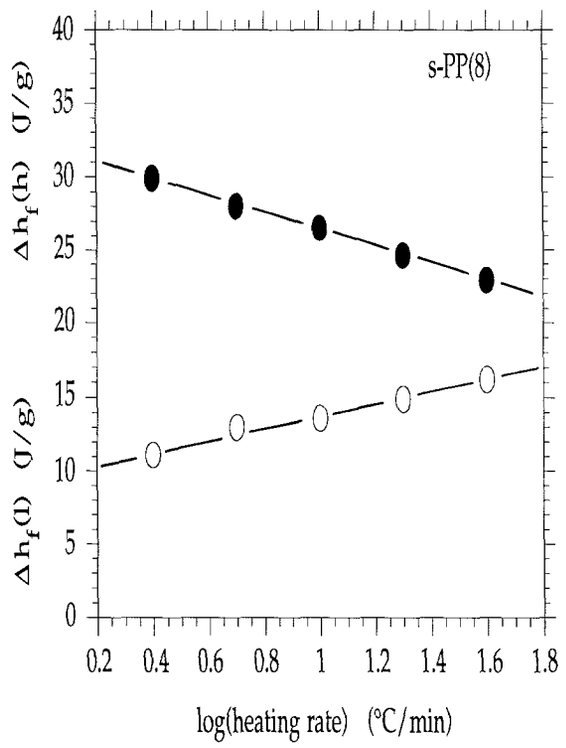

Figure 6 Relationships between the heats of fusion of the melting peaks and the logarithmic heating rate for s-PP(8) after isothermal crystallization at 80°C: (○) low-melting peak; (●) high-melting peak

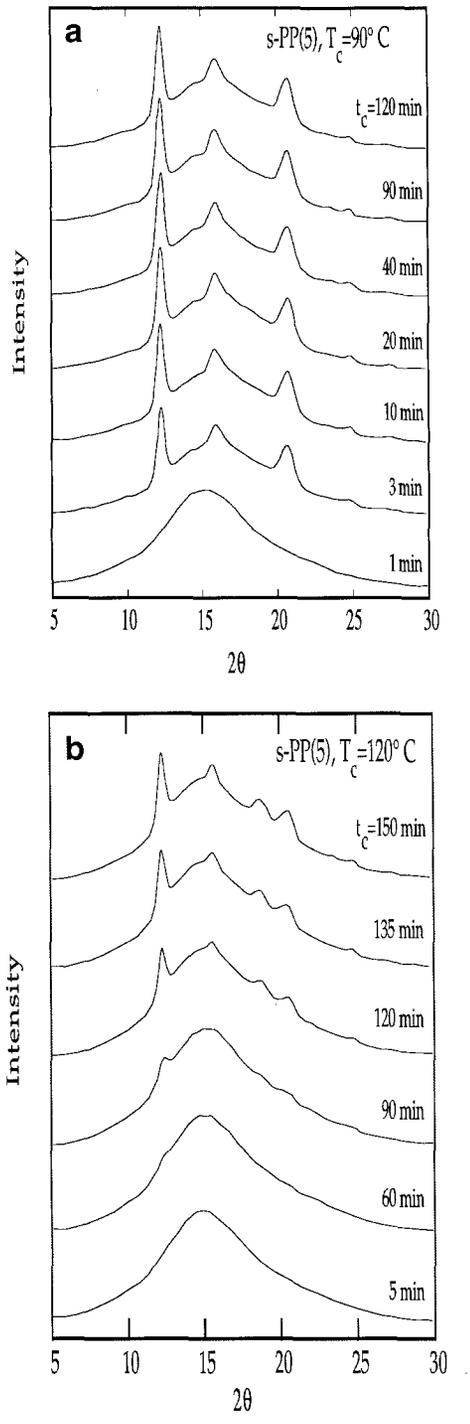

Figure 7 Set of time-resolved WAXD patterns for s-PP(5) isothermally crystallized at (a) 90°C and (b) 120°C over the indicated times

isothermally after heating. A clear exothermic peak can be detected, indicating a recrystallization process. For s-PP(5), for example, after it was completely crystallized at 90°C the sample was heated up at a heating rate of 10°C min^{-1} to 128°C, and then it was held at that temperature. A clear exothermic process was recorded within a few minutes with a heat of crystallization of less than 1 kJ mol^{-1}. If the sample was isothermally crystallized at 128°C from the melt, over a few hundred minutes were necessary to develop the crystallinity.

Structural changes during crystallization and melting

Structural changes during heating were detected from WAXD experiments for these fractions under the same isothermal crystallization conditions and heating rates after crystallization as reported for the d.s.c. experiments. *Figures 7a* and *7b*, respectively, depict the time-resolved WAXD patterns of s-PP(5) during isothermal crystallization at 90°C and 120°C. It is interesting that in the crystal development at 90°C, only three major WAXD diffraction peaks are seen, and that these are superimposed on a very prominent, amorphous-like background even after prolonged crystallization. These three peaks correspond to a typical s-PP pattern with (200), (020) and (220, 121) reflection planes (these assignments are based on the doubled unit cell[18–23]; otherwise, they should be (200), (010) and (210, 111) planes). No trace of a peak at $2\theta = 18.8°$ is observed (which would have confirmed the regularly antichiral, doubled unit cell). When the isothermal crystallization temperature increases to 120°C, the WAXD patterns show that even in the beginning of the crystal development the reflection peak at $2\theta = 18.8°$ appears together with the other three major reflection peaks (*Figure 7b*). This peak has been assigned to the (211) planes after Lovinger *et al.*[19,23], and confirms the fully antichiral packing (cell III). From *Figures 7a* and *7b* it can be seen that the crystalline reflection (peaks) intensities in the WAXD patterns increase continuously, while the amorphous background decreases. *Figures 8a* and *8b* show a parallel study of WAXD patterns for s-PP(8) crystallized at 90°C and 115°C. Similar trends are found as in the case of s-PP(5). However, one apparent difference is that for this fraction the peak intensity at $2\theta = 18.8°$ is not as great as in the s-PP(5) sample of relatively low molecular weight.

The WAXD patterns can also provide useful information about crystallinity and apparent crystal size. *Figure 9* illustrates crystallinity data for s-PP(3) and s-PP(8) fractions crystallized at different temperatures. It should be noted that these are not traditional crystallinity indices because the 'amorphous peak' also incorporates the positional packing disorder of s-PP fractions; that is, the 'streaks' reported by Lovinger *et al.*[5,19,23] in electron diffraction patterns would be indistinguishable from the amorphous background in an unoriented specimen such as used here. With increasing crystallization temperature, crystallinity increases only minimally for each fraction to ca. 115°C, and then the rate of increase above that temperature is different based on molecular weight. While the crystallinity of the higher molecular weight s-PP(8) is ca. 10% below the corresponding value for s-PP(3) at an equivalent crystallization temperature (approximately 3°C difference in undercooling), its increase in crystallinity above 115°C is slower.

Turning to the apparent crystal sizes calculated using the Scherrer equation, as shown in *Figure 10*, below ca. $T_c = 100°C$ for s-PP(5), s-PP(7) and s-PP(9) as examples, it is interesting to note that with decreasing crystallization temperature and increasing molecular weight the apparent crystal sizes decrease. The high molecular weight fraction shows lower apparent crystal size compared to the lower molecular weight samples at the same crystallization temperature (undercooling). Furthermore, a clear drop in the sizes for the (200) and (020) crystalline plane is found in a crystallization temperature range between 100 and 110°C for these fractions. Further raising the temperature above ca. 120°C leads to a continuous increase of the apparent

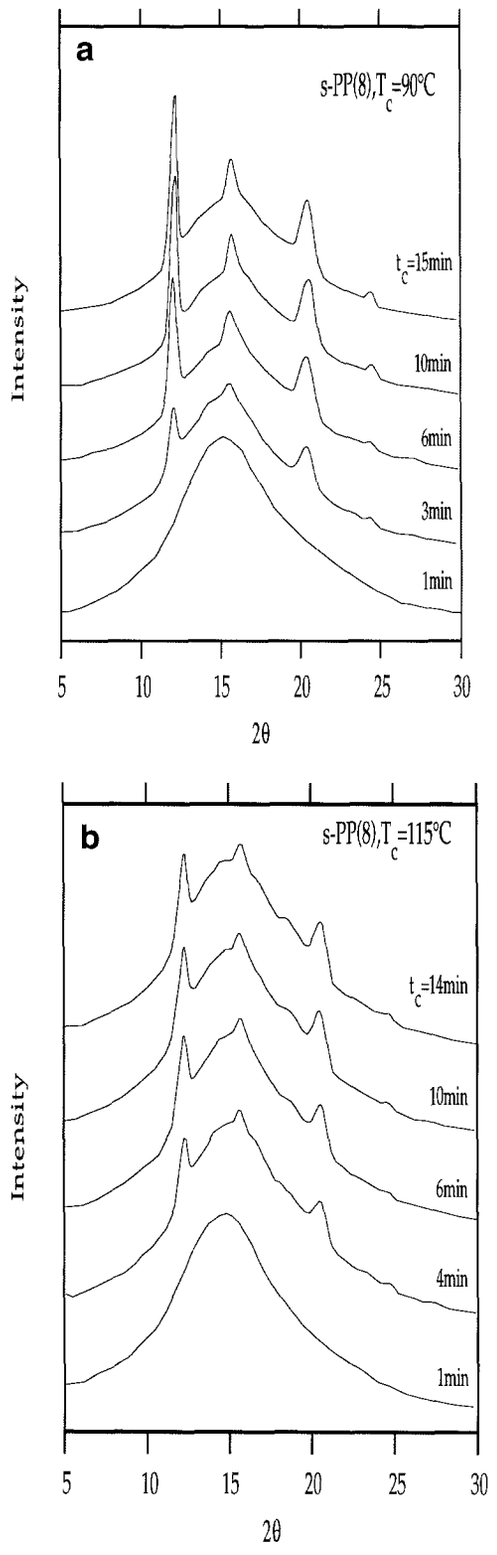

Figure 8 Set of time-resolved WAXD patterns for s-PP(8) isothermally crystallized at (a) 90°C and (b) 115°C over the indicated times

crystal sizes again. This behaviour is atypical in the field of polymer crystallization. With increasing molecular weight, this drop is expected to vanish gradually.

WAXD continuous heating experiments were also conducted for s-PP(3) at a constant heating rate of 2°C min^{-1} after isothermal crystallization at 90°C (see *Figure 7*). *Figure 11* shows that when the temperature is raised by 20–25°C above the crystallization temperature crystals start melting, as inferred from the slight reduction in the WAXD intensities. After the temperature reaches

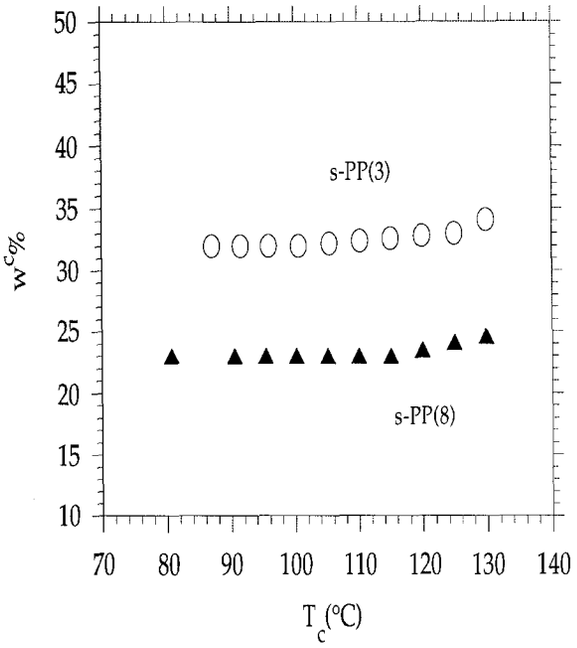

Figure 9 Relationships between crystallinity and crystallization temperature for s-PP(3) and s-PP(8)

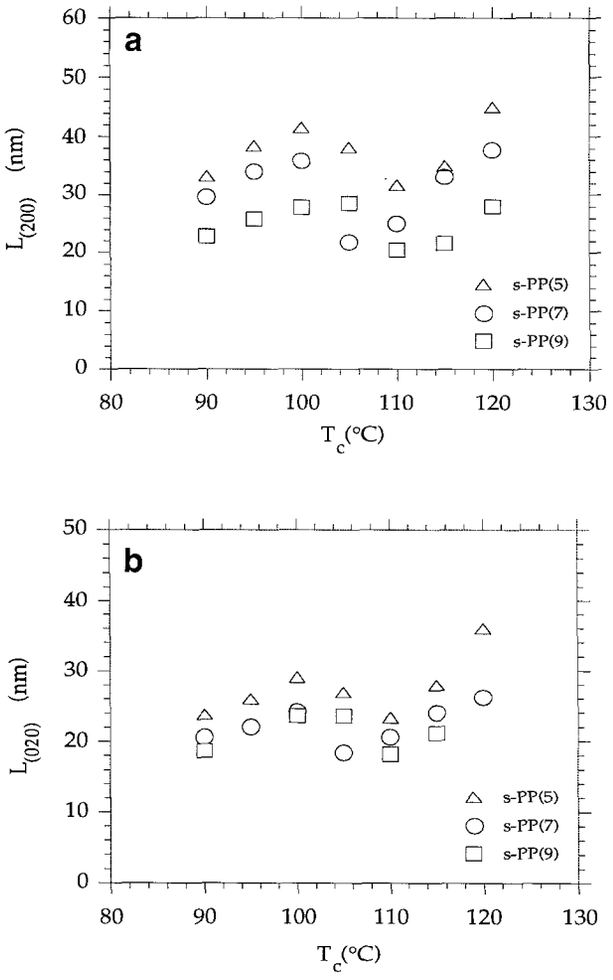

Figure 10 Relationships between apparent crystal size of (a) (200) and (b) (020) planes and crystallization temperature for s-PP(5), s-PP(7) and s-PP(9)

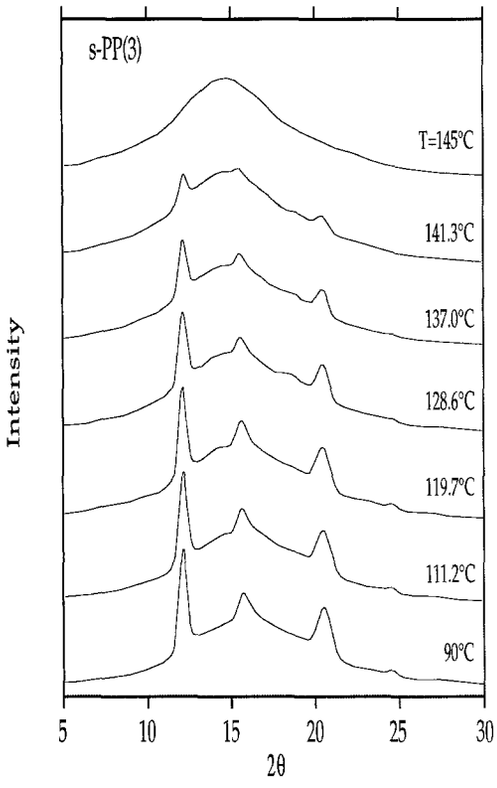

Figure 11 Set of WAXD patterns collected during continuous heating at 2°C min^{-1} for s-PP(3) after isothermal crystallization at 90°C

its value at the end of the first melting peak (ca. 128°C), a recrystallization process leads to newly developed crystals which show a new peak at $2\theta = 18.8°$. Only when the temperature exceeds that of the second melting peak does the crystal become totally molten and an amorphous halo is seen. Further experiments carried out by holding the temperature between the two melting peaks (in the same way as for the d.s.c. experiments described earlier) showed that the recrystallization process is more pronounced, with a clear reflection peak at $2\theta = 18.8°$.

DISCUSSION

Crystallization kinetics

As shown in *Figures 1* and *2*, the overall crystallization kinetics of the s-PP fractions seems to follow the general pattern of polymer crystallization. However, a special feature in *Figure 2* is the discontinuity of the slopes in the plot at a constant undercooling of about 50°C for both fractions. Furthermore, the ratios of these two slopes are close to 2. This discontinuity may very likely reflect a regime III to regime II transition as proposed by nucleation theory[39–43]. Compared with the surface free energies of i-PP obtained in a similar procedure (for i-PP with a relatively high isotacticity, the fold surface free energy is around 55–65 erg cm^{-2} and the lateral surface free energy is around 11–12 erg cm^{-2})[33,34], the product of the fold and lateral surface free energies of s-PP would be around 418–500 erg^2 cm^{-4}, which is about 63–75% of that in the i-PP case. This estimate is different from that obtained through linear crystal growth rate observations at a relatively high crystallization temperature reported earlier by Miller and Seeley[28], where a value of 208–256 erg^2 cm^{-4} was found under regime II growth assumptions. This is due to the difference in the equilibrium heat of fusion used in their calculation (their 3.14 kJ mol^{-1} *versus* our 8.0 kJ mol^{-1}). If we use 8.0 kJ mol^{-1} as the equilibrium heat of fusion to recalculate Miller and Seeleys' data, the product will be 482 erg^2 cm^{-4}. It was predicted by Clark and Hoffman that at around $\Delta T = 50°C$ a regime III to regime II transition should be observed for s-PP[45]. This prediction fits well with the experimental observations reported here. Since all of these s-PP fractions possess a similar syndiotacticity (*Table 1*), the overall crystallization rate difference among these fractions should truly reflect the molecular weight dependence, as shown in *Figure 2*. From the low molecular weight side, the overall crystallization rate decreases with increasing molecular weight up to about 50 000. Further increasing the molecular weight leads to little change in the overall crystallization rate. A detailed discussion of the molecular weight dependence in this series of s-PP fractions will be given elsewhere[46].

Antichiral packing in the crystals

The appearance of the X-ray peak at $2\theta = 18.8°$ has been attributed to the fully antichiral packing along both the *a* and *b* axes of the crystal, as suggested by Lovinger *et al.*[5,19–22]. In this study, we have observed that the intensity of this peak is not only dependent upon crystallization temperature, but is also associated with molecular weight (*Figures 7* and *8*). This indicates that the antichiral packing in the s-PP crystals with a doubled unit cell may indeed be controlled through crystallization kinetics as suggested earlier[5,20,21]. Only when a chain molecule with the opposite handedness deposits directly on top of a chain on the crystal growth front along the (010) plane[19,21] can the doubling of the unit cell be obtained. The selection of the opposite handedness in chain molecules should be determined by the competition between the crystallization rate (*Figures 1* and *2*) and the molecular motion, and should therefore be both temperature and molecular weight dependent. Decreased molecular mobility caused either by high molecular weight (chain entanglements) and/or fast crystallization (low crystallization temperature) may lead to a relatively random selection of the handedness of chain packing in the crystals, which would thus detract from the trend for a regular antichiral arrangement. The role of chain entanglements is also reflected through the decrease in the apparent crystallinity with increasing molecular weight (*Figure 9*). It seems that in a crystallization temperature range around 100 to 110°C the s-PP fractions undergo a transition from a more or less random handedness packing to the fully antichiral packing.

The most striking experimental observation is the discontinuity in the change in apparent crystal size with crystallization temperature, as shown in *Figure 10*. It is surprising that the temperature of this discontinuity approximately corresponds with the temperature of disappearance of the double melting peaks. Since the apparent crystal size calculated by using the Scherrer equation is a representation of the correlation length normal to a family of crystalline planes, the apparent crystal size should increase with increasing crystallization temperature. This has been observed in many crystalline polymers, and the nearest system related to this case is in i-PP fractions reported several years ago[33]. Our explanation of this exceptional departure in s-PP is based on the change in crystal structure with crystallization temperature. Below the crystallization temperature range

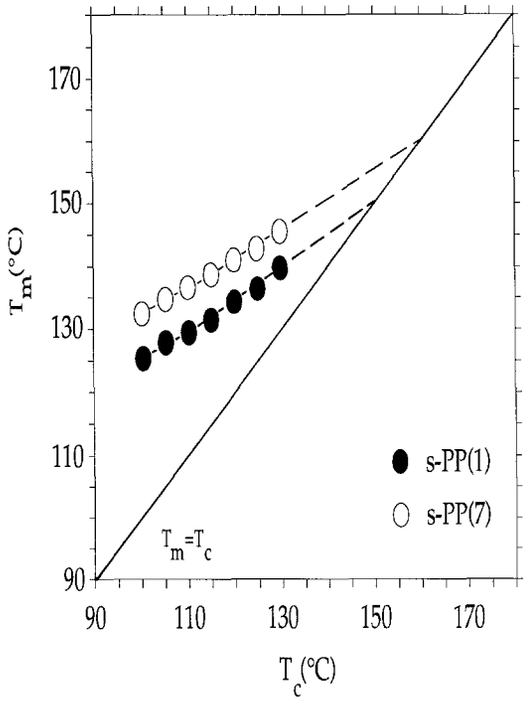

Figure 12 Relationships between melting temperature and crystallization temperature for s-PP(1) and s-PP(7)

of about 100 to 110°C, WAXD indicates that no pure antichiral packing is seen (no doubled cell reflection at 18.8°). Statistical departures from the regular antichiral packing with more or less random handedness should impose less restriction to the correlation length of the crystal. However, above this temperature range, a fully antichiral packing along both axes is evident from the X-ray patterns, so that opposite handedness is necessary in this case. As a result, a more restricted and, therefore, a shorter correlation length may be generated compared to that at low crystallization temperatures. Only upon further increase in crystallization temperature can this correlation length be enhanced again, as shown in *Figure 10*.

The origin of the two melting peaks

From our d.s.c. and WAXD experiments (*Figures 3, 4, 6* and *11*), it seems that the high-melting peak is most likely formed through reorganization and/or a melt-recrystallization process during heating when two melting peaks are observed[47]. For higher molecular weights, this effect is increasingly hampered due to reduced chain mobility and enhanced entanglements. When the crystallization temperature increases from the low to the intermediate region, the low-melting peak shows an increase in its heat of fusion. This may be an indication that the crystal becomes progressively more perfect as the temperature is raised (*Figures 3, 4* and *6*). On the other hand, these two melting peaks seem to correspond well to two distinct crystal packings as described above, namely the low-melting peak may be attributed to the less extensive and more defective antichiral packing (cell II), while the high-melting peak may be attributed to an antichiral packing along both the *a* and *b* axes[19,21]. If these structural assignments are correct, the transformation from cell II to cell III must be a result of reorganization and melt-recrystallization processes during heating. One should note that a change in handedness does not necessarily need melt recrystallization, as has been shown for i-PP and other vinyl polymer crystals. In the case of i-PP, only the change in up and down inclinations of the methyl groups has to involve large-scale molecular motion. A molecule must be inverted to change the inclination of methyl groups with respect to the chain axis. However, this is not the case in s-PP since there is no directionality to its $(t_2g_2)_2$ conformation. When the molecular weight increases, the crystal becomes increasingly resistant to effective annealing towards higher-melting forms. As a result, a larger portion of the low-melting material remains during heating of high molecular weight materials. We thus expect that with increasing molecular weight the melt-recrystallization process will become more predominant and effective compared to the reorganization process. However, further detailed investigation is necessary to achieve a full understanding of the transformations between these two melting peaks.

It is interesting to note that the change from two melting peaks to a single melting peak and the discontinuity in the variation of the apparent crystal size occur around the temperature region where the regime II to regime III transition occurs. Detailed connections between these behaviours are not clear at this moment.

Thermodynamic equilibrium properties

If one uses a Hoffman–Weeks plot to obtain the extrapolated equilibrium melting temperature T_m° for each fraction, very reasonable T_m *versus* T_c relationships are obtained, as shown for example in *Figure 12* for s-PP(1) and s-PP(7). It is very important to use the correct melting temperatures for the extrapolation based on the change in crystal size. The data used here represent the peak melting temperatures for each fraction after extrapolation to a $0°C\,min^{-1}$ heating rate, as described above (see *Figure 5*). Note that only the low-melting peak temperatures are used. After the extrapolations for all the fractions, it is seen that T_m° is molecular weight dependent. For s-PP(1), the value is 148°C, followed by a T_m° of 155°C for s-PP(2). After the molecular weight exceeds 40 000, the extrapolated equilibrium melting temperature becomes constant at 160°C for a dyad syndiotacticity of $94\pm1\%$ (pentad syndiotacticity of $86\pm1\%$; *Table 1*). It should be pointed out that the relationships between T_m and T_c in *Figure 12* are not exactly linear, and the melting temperature increments with crystallization temperature at the low T_c side are not as large as those at the high T_c side. It is also important that T_m° is a very sensitive function of the degree of syndiotacticity. For a 99% dyad sample, actual melting temperatures as high as 163°C were obtained[23].

Another approach to obtain the equilibrium melting temperature is based on a relationship between melting temperature and reciprocal lamellar thickness. The former is the same as that used in the T_m *versus* T_c plot, while the latter comes from SAXS experiments after applying the appropriate correlation function method to obtain the lamellar thickness[34]. *Figure 13* illustrates the relationships for two of the fractions studied. It is clear that if we use the low-melting peak temperature the results are consistent with the data obtained through the Hoffman–Weeks plot (*Figure 12*), giving an equilibrium melting temperature of 160 ± 1°C for the s-PP fraction with a dyad syndiotacticity of 94% when the molecular

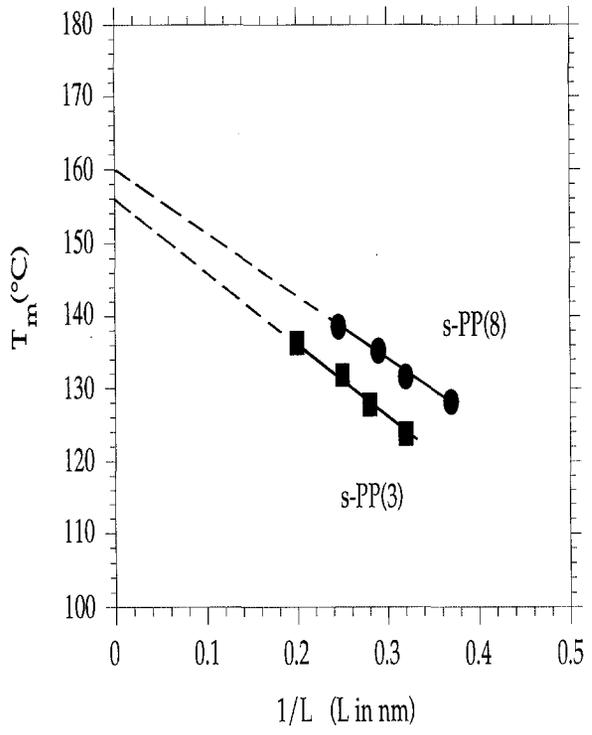

Figure 13 Relationships between melting temperature and reciprocal lamellar thickness for s-PP(3) and s-PP(8)

weight exceeds about 50 000. Further analysis leads to a numerical value for the fold surface free energy based on the slope of the relationship in *Figure 13*. The value ranges from 46 erg cm^{-2} for s-PP(8) to 55 erg cm^{-2} for s-PP(3). These values are relatively low compared to the fold surface free energy of i-PP[35]. If one assumes that the fold surface free energy obtained from the melting data can be used to analyse the product of the fold and lateral surface free energies derived from the kinetic data, the lateral surface free energy of s-PP fractions thus ranges from 8 to 10 erg cm^{-2}. Another way[39–42] to estimate the lateral surface free energy is through the relationship $\sigma = 0.1(ab)^{1/2}\Delta h_f$. The calculated value is then 11.2 erg cm^{-2}. The range for this value is close to the corresponding ranges for i-PP[45] and polyethylene[39,40]. Such a fold surface free energy is about 76–84% of that in i-PP fractions. In an earlier study, Clark and Hoffman[45] reported that the fold surface free energy should be around 50 erg cm^{-2}, which is close to the experimental result obtained in this work. This value is substantially higher than that of the much more flexible poly(ethylene oxide) fractions[48].

For the equilibrium heats of fusion of these s-PP fractions, one may use the crystallinity data obtained from WAXD experiments and combine them with the heat of fusion data from d.s.c. Each of the heats of fusion is measured at a different heating rate. At fast heating rates the heat of fusion reaches almost a constant which is independent of the heating rate. One assumes that this heat of fusion does not involve an annealing effect during heating, and it is used in the extrapolation between the crystallinity and the heat of fusion. This extrapolation indicates that the heat of fusion for 100% crystallinity reaches 8.0 ± 0.3 kJ mol^{-1} (average of seven fractions of molecular weight higher than 20 000). Note that this heat of fusion excludes the contribution of defective crystals with the positional packing disorder in the unoriented samples.

An important issue is that the lamellar thicknesses in these samples range between 2.5 and 5 nm, depending upon crystallization temperature and molecular weight. When one estimates the number-averaged syndiotactic block in *Table 1*, it is between 29 and 37 repeat units. In the unit cell, the *c* axis (0.740 nm) consists of four repeat units. As a result, the length of the number-averaged syndiotactic block ranges from 5.4 to 6.8 nm. This may be an indication that no defects should be included in the crystal lattice. However, a detailed conformational analysis of defects must be carried out before a quantitative defect inclusion or exclusion model[49–53] can be proposed.

CONCLUSIONS

Based on d.s.c., WAXD and SAXS experimental observations, it is evident that the equilibrium melting temperature of this series of s-PP fractions (94% racemic dyads) at sufficiently high molecular weight is 160 ± 1°C with an equilibrium heat of fusion of 8.0 ± 0.3 kJ mol^{-1}. The overall crystallization rate decreases with increasing molecular weight at the same undercooling below a molecular weight of 50 000. A discontinuity of the slope was observed in the kinetic study based on a conventional nucleation theory plot, which may be associated with a regime III to regime II transition. The double melting peak phenomenon can be associated with the chain-packing changes in the crystal structure based on the development of a reflection peak at $2\theta = 18.8°$ detected via WAXD experiments and assigned by Lovinger *et al.* to a transition towards full antichiral packing and doubling of the unit cell. These chain-packing changes are dependent not only on crystallization temperature but also on molecular weight, reflecting the effects of chain mobility and entanglements in these s-PP fractions.

ACKNOWLEDGEMENTS

This work was supported by S.Z.D.C.'s Presidential Young Investigator Award from the National Science Foundation (DMR-9157738), the Exxon Education Foundation, and Phillips Petroleum Company.

REFERENCES

1 Natta, G., Pasquon, I., Corradini, P., Peraldo, M., Pegoraro, M. and Zambelli, A. *Rend. Accad. Naz. Lincei* 1960, **28**, 539
2 Natta, G., Pasquon, I. and Zambelli, A. *J. Am. Chem. Soc.* 1962, **84**, 1488
3 Zambelli, A., Natta, G. and Pasquon, I. *J. Polym. Sci. (C)* 1963, **4**, 411
4 Corradini, P., Natta, G., Ganis, P. and Temussi, P. A. *J. Polym. Sci. (C)* 1967, **16**, 2477
5 Lotz, B., Lovinger, A. J. and Cais, R. E. *Macromolecules* 1988, **21**, 2375
6 Youngmann, E. A. and Boor, J. *Macromol. Rev.* 1967, **2**, 33
7 Grant, I. J. and Ward, I. M. *Polymer* 1965, **6**, 223
8 Inagaki, H., Miyamoto, T. and Ohta, S. *J. Phys. Chem.* 1966, **70**, 3420
9 Gee, D. R. and Melia, T. P. *Polymer* 1969, **10**, 239
10 Tadokoro, H., Kobayashi, M., Kobayashi, S., Yasufuki, K. and Mori, K. *Rep. Prog. Polym. Phys. Jpn* 1966, **9**, 181
11 Boor, J. and Youngmann, E. A. *J. Polym. Sci. (A-1)* 1966, **4**, 1861
12 Haftka, S. and Konnecke, K. *J. Macromol. Sci., Phys. B* 1991, **30**, 319

13 Boor, J. and Youngmann, E. A. *J. Polym. Sci. (B)* 1965, **3**, 577
14 Ferguson, R. C. *ACS Polym. Prepr.* 1967, **8** (2), 1026
15 Ferguson, R. C. *Trans. N. Y. Acad. Sci.* 1967, **29**, 495
16 Heatley, F. and Zambelli, A. *Macromolecules* 1969, **2**, 618
17 Tonelli, A. E. and Schilling, F. C. *Acc. Chem. Res.* 1981, **14**, 233
18 Galambos, A., Wolkowicz, M., Zeigler, R. and Galimberti, M. *ACS Polym. Mater. Sci. Eng.* 1991, **64**, 45
19 Lovinger, A. J., Lotz, B. and Davis, D. *ACS Polym. Prepr.* 1992, **33** (1), 270
20 Lovinger, A. J., Davis, D. and Lotz, B. *Macromolecules* 1991, **24**, 552
21 Lovinger, A. J., Lotz, B., Davis, D. D. and Padden Jr, F. J. *Macromolecules* 1993, **26**, 3494
22 Lovinger, A. J., Lotz, B. and Davis, D. *Polymer* 1990, **31**, 2253
23 Lovinger, A. J., Lotz, B. and Davis, D. D. *Macromolecules* 1993, **26**, 3494
24 Turner-Jones, A. and Cobbold, A. J. *J. Polym. Sci. (B), Polym. Lett.* 1968, **6**, 539
25 Natta, G., Peraldo, M. and Allegra, G. *Makromol. Chem.* 1964, **75**, 215
26 Chatani, Y., Maruyama, H., Noguchi, K., Asanuma, T. and Shiomura, T. *J. Polym. Sci. (C), Polym. Lett.* 1990, **28**, 393
27 Chatani, Y., Maruyama, H., Asanuma, T. and Shiomura, T. *J. Polym. Sci., Polym. Phys. Edn* 1991, **29**, 1649
28 Miller, R. L. and Seeley, E. G. *J. Polym. Sci., Polym. Phys. Edn* 1982, **20**, 2297
29 Miller, R. L. *J. Polym. Sci.* 1962, **57**, 975
30 Natta, G., Corradini, P. and Ganis, P. *Makromol. Chem.* 1960, **39**, 238
31 Marchetti, A. and Martuscelli, E. *J. Polym. Sci. (A-2)* 1974, **12**, 1649
32 Koningsveld, R. and Staverman, A. J. *Adv. Polym. Sci.* 1968, **7**, 1
33 Cheng, S. Z. D., Zhang, A.-Q., Chen, J.-H., Barley, J. S., Habunshuss, T. and Zuchack, P. *Macromolecules* 1991, **24**, 3937
34 Tanabe, Y., Strobl, G. R. and Fischer, E. W. *Polymer* 1985, **27**, 1147
35 Cheng, S. Z. D., Janimak, J. J., Zhang, A.-Q. and Hsieh, E. T. *Polymer* 1991, **32**, 648
36 Janimak, J. J., Cheng, S. Z. D., Giusti, P. A. and Hsieh, E. T. *Macromolecules* 1991, **24**, 2253
37 Janimak, J. J., Cheng, S. Z. D., Zhang, A.-Q. and Hsieh, E. T. *Polymer* 1992, **33**, 728
38 Hsieh, E. T. and Chu, P. personal communication, 1993
39 Hoffman, J. D., Davis, G. T. and Lauritzen, Jr, J. I. in 'Treatise on Solid State Chemistry' (Ed. N. B. Hannay), Vol. 3, Plenum Press, New York, 1976, Ch. 7
40 Hoffman, J. D. *Polymer* 1982, **23**, 656
41 Hoffman, J. D. *Polymer* 1983, **24**, 3
42 Hoffman, J. D. and Miller, R. L. *Macromolecules* 1988, **21**, 3038
43 Hoffman, J. D., Miller, R. L., Marand, H. and Roitman, D. B. *Macromolecules* 1992, **25**, 2221
44 Illiers, K.-H. *Eur. Polym. J.* 1974, **10**, 911
45 Clark, E. J. and Hoffman, J. D. *Macromolecules* 1984, **17**, 878
46 Rodriguez, J., Cheng, S. Z. D., Hsieh, E. T. and Chu, P. in preparation
47 Wunderlich, B. 'Macromolecular Physics', Vol. 3, Academic Press, New York, 1980, Ch. 9
48 Cheng, S. Z. D., Chen, J.-H. and Janimak, J. J. *Polymer* 1990, **31**, 1081
49 Flory, P. J. *Trans. Faraday Soc.* 1955, **51**, 848
50 Sanchez, I. C. and Eby, R. K. *J. Res. Natl Bur. Stand., Sect. A* 1973, **77**, 353
51 Sanchez, I. C. and Eby, R. K. *Macromolecules* 1975, **8**, 639
52 Fischer, E. W., Sterzel, H. J. and Wegner, G. *Kolloid Z. Z. Polym.* 1973, **251**, 980
53 Helfand, E. and Lauritzen Jr, J. I. *Macromolecules* 1973, **6**, 631